Thin Solid Films 518 (2010) 5300–5303

Contents lists available at ScienceDirect

Thin Solid Films

journal homepage: www.elsevier.com/locate/tsf

Formation and magnetization reversal mechanisms of nano-size Fe arrays prepared on anodic aluminum oxide templates

Kai-Tze Huang [a,b], Po-Cheng Kuo [a], Ger-Pin Lin [a], Chih-Lung Shen [a], Yeong-Der Yao [c,*]

[a] Institute of Materials Science and Engineering, National Taiwan University, Taipei 10617, Taiwan
[b] Institute of Physics, Academia Sinica, Taipei 11529, Taiwan
[c] Institute of Applied Science and Engineering, Fu Jen University, Taipei 24205, Taiwan

ARTICLE INFO

Article history:
Received 21 February 2009
Received in revised form 3 April 2010
Accepted 8 April 2010
Available online 6 May 2010

Keywords:
Anodic aluminum oxide
Nanostructure array
Scanning Electron Microscopy
Magnetization reversal
Magnetic Force Microscopy
Magnetic storage media

ABSTRACT

Vertically aligned Fe arrays have been self-assembled on anodic aluminum oxide templates by evaporation. The rims of the pores, which act as obstacles to the stacking of atoms, prevent them from forming continuous films. By controlling the Fe nominal thicknesses (τ_n) from 400 to 5 nm, the morphology is changed from continuous film to isolated arrays, leading to the change of the predominant magnetization reversal from domain wall motion to spin rotation. For samples with τ_n<59 nm, isolated, rather than interconnected, morphology is formed. In this range, the coercivity shows a spectacular change for τ_n = 47 nm, with an array diameter of about 52 nm, achieving a maximum of about 38 kA/m. The critical dimension of single-domain array is therefore determined. The magnetostatic and exchange interactions are reduced due to the thermal fluctuation, and the magnetization leaves from the in-plane direction to be randomly distributed in 3-D, for τ_n<27 nm.

1. Introduction

Recently, nano-size magnetic arrays with different shapes, such as nanodots, nanorods or nanowires [1–5], have attracted much attention due to potential applications in storage because reduced dimensions match the demand for increasing the areal density. Furthermore, the isolated morphology reduces the inter-array exchange interaction, resulting in acceptable signal-to-noise ratio. Research on granular magnetic films, in which grains are separated and refined by non-magnetic materials, such as MgO, Si_3N_4, SiO_2, Al_2O_3, and TiO_2 [6–10], are also widely reported for these purposes. However, no research to date has been reported on nano-size magnetic arrays directly formed on the top of nanoporous anodic aluminum oxide (AAO) template without complicated fabrication processes or addition of non-magnetic materials. Eliminating these steps provides the benefits of low cost, large area, and good isolation in forming nano-size magnetic arrays.

In general, if atoms are directly deposited on an AAO template, they stack up and form continuous films [11,12]. In our previous research, nano-size Pt arrays with isolated morphology were fabricated on AAO templates by magnetron sputtering, following the restriction mechanism [13]. In this study, the specific surface sites of AAO templates are utilized for the nucleation and growth of stacked atoms to form nano-size Fe arrays. The size-dependent magnetization reversal is investigated for various thicknesses of the Fe arrays. The Fe thickness generally relates to the effective deposition time which is a linear relation that has been calibrated; hence, it is defined as the Fe nominal thickness (τ_n).

2. Experiment

The ferromagnetic element Fe, which can be easily and reproducibly prepared for analysis of fundamental magnetic properties, was evaporated on commercially available AAO templates with a pore diameter of about 75 nm and a pore aspect ratio (pore depth : pore diameter) of about 400:1 (as per AAO75 in Ref. [13]), forming nano-size magnetic arrays. The deposition source was iron coils with a purity of 99.995%. Evaporation was performed at a rate of about 0.4 nm/h in an ultra-high vacuum chamber with a base pressure of 2×10^{-7} Pa. Before Fe array deposition, the AAO templates were cleaned by Ar^+ ion bombardment. The magnetization reversal of the Fe arrays was measured using a vibrating sample magnetometer (model 7407, Lake Shore Inc.) at room temperature with a maximum applied field and a minimum sensitivity of 1600 kA/m and 10^{-8} A m^2, respectively. A scanning electron microscope (SEM, model S-4200, Hitachi Co.) with an operating voltage of 15 kV and a magnetic force microscope (MFM, model Solver-P47, NT-MDT Co.) were used to

* Corresponding author. Tel.: +886 2 27896717; fax: +886 2 27834187.
E-mail address: ydyao@phys.sinica.edu.tw (Y.-D. Yao).

0040-6090/$ – see front matter © 2010 Elsevier B.V. All rights reserved.
doi:10.1016/j.tsf.2010.04.020

identify the morphology and domain structure of the stacked Fe atoms, respectively.

3. Results and discussion

Fig. 1 shows a plane-view SEM image of nano-size Fe arrays prepared in various nominal thicknesses. With increases in the Fe nominal thickness, the average diameter and morphology vary from about 26 nm with isolation for $\tau_n = 12$ nm to about 87 nm with interconnection for $\tau_n = 84$ nm, respectively. Interconnected morphology is observed for $\tau_n > 59$ nm. In Fig. 1(a), which shows the results for $\tau_n = 12$ nm, isolated arrays are observed just on the corner regions between the pores, or certain regions with large areas, and the restriction mechanism is confirmed [13]. The arrays are lengthened due to further deposition. A few atoms are also stacked on the perimeters of the arrays, leading to coarsening, but very few fill in the vacant spaces [11,14]. About the shadowing effect, Lei et al. [14] found that the amount of atoms filling the vacant spaces varies according to the pore aspect ratio of the AAO template. Pores with a high aspect ratio lead to the majority of the atoms being stacked on the perimeter. This is confirmed in the current study, the AAO template, which has pores with a high aspect ratio of about 400:1, results in the deposited Fe atoms to be stacked on the perimeter of the pores, close to the surface. The amount of atoms, stacked on the inner-wall, is known to decrease as the depth increases [11,14,15]. Moreover, as the nominal thickness of nano-size Fe arrays increases, the pores are blocked out, further deposition of atoms in the pores are being obstructed, as shown in Fig. 1(f). The oxidation of these small amounts of stacked Fe atoms, forming anti-ferromagnetic oxide films with a thickness of about 3 to 5 nm, can lower the contribution to the magnetization reversal, which is dominated by the nano-size Fe arrays on the top of AAO template. In addition, Li et al. [16] found that the oxide shell of an isolated array contributes to the reduction of the inter-array exchange interaction.

The normalized in-plane and out-of-plane hysteresis loops of nano-size Fe arrays with various nominal thicknesses of 12 nm, 27 nm, 47 nm, and 400 nm, obtained in an applied field of 1600 kA/m, are shown in Fig. 2. As shown in Fig. 2(a) and (b), the hysteresis loops of the $\tau_n = 12$ and 27 nm samples show a nearly random-distributed magnetization. Lower ratios of coercivity over saturation field (H_c/H_s) of about 0.126 and 0.131, compared to that of about 0.195 for $\tau_n = 47$ nm sample (shown in Fig. 2(c)), are achieved, which is consistent with the corresponding SEM images. The low inter-array exchange interaction, resulting from the isolated morphology, leads an increased saturation field. Due to the independent rotation, the high switching field distribution is therefore achieved. As the Fe nominal thickness increases to 400 nm, the magnetization gradually changes to the in-plane direction. The easy direction of the sample can be verified by the ratio of out-of-plane squareness over in-plane squareness ($S_\perp/S_\parallel$), where the squareness (S) is defined as remanent magnetization over saturation magnetization (M_r/M_s). Accordingly, the magnetization, preferring the in-plane direction, is verified by the ratio of $S_\perp/S_\parallel < 1$, especially for $\tau_n > 27$ nm, as shown in Fig. 3(a). Furthermore, for $\tau_n = 400$ nm, an in-plane hysteresis loop with small coercivity, resembling that of the continuous film, is obtained, as shown in Fig. 2(d). This indicates that the magnetization reversal is close to that of continuous film, but the pores, beneath the cover of Fe atoms, lower the in-plane squareness and impede the cooperative rotation.

The in-plane and out-of-plane coercivity of nano-size Fe arrays is plotted as a function of the Fe nominal thickness in Fig. 3(b). In previous research [17], the coercivity was varied by the size of the multi-domain particles. An increase in coercivity of fine particles, especially single-domain particles, was achieved. As the particle diameter falls below the critical size of the single domain, the thermal stability ratio (K_uV/k_BT) is decreased proportionally to the particle

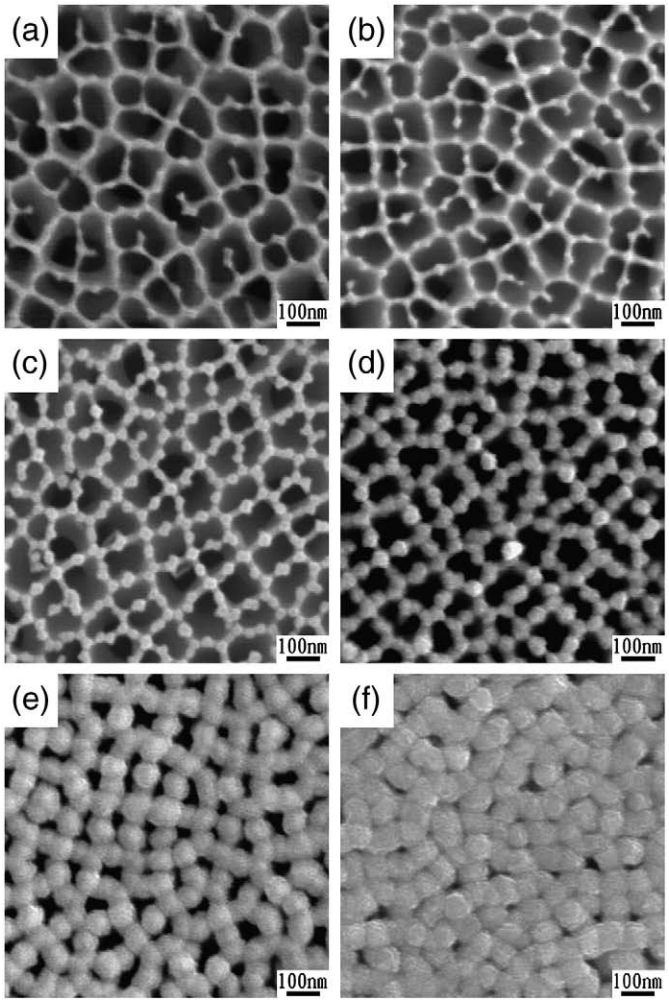

Fig. 1. Plane-view SEM images of nano-size Fe arrays with various nominal thicknesses of (a) 12 nm, (b) 27 nm, (c) 47 nm, (d) 59 nm, (e) 71 nm, and (f) 84 nm.

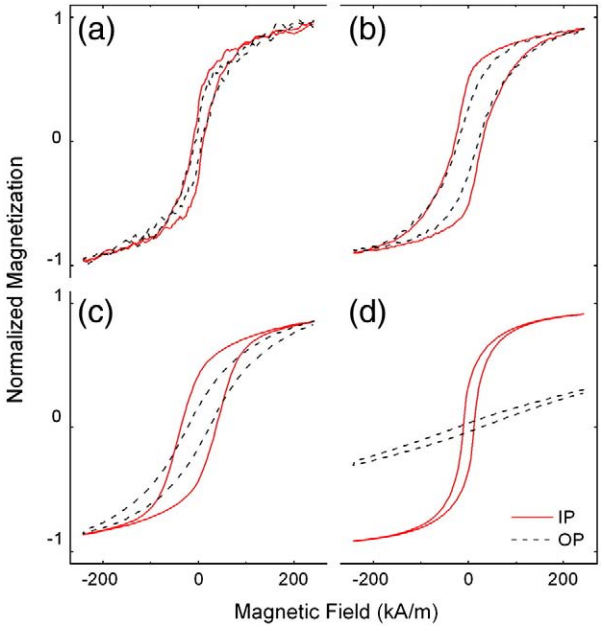

Fig. 2. The normalized in-plane (IP) and out-of-plane (OP) hysteresis loops of nano-size Fe arrays in an applied field of 1600 kA/m with various nominal thicknesses of (a) 12 nm, (b) 27 nm, (c) 47 nm, and (d) 400 nm.

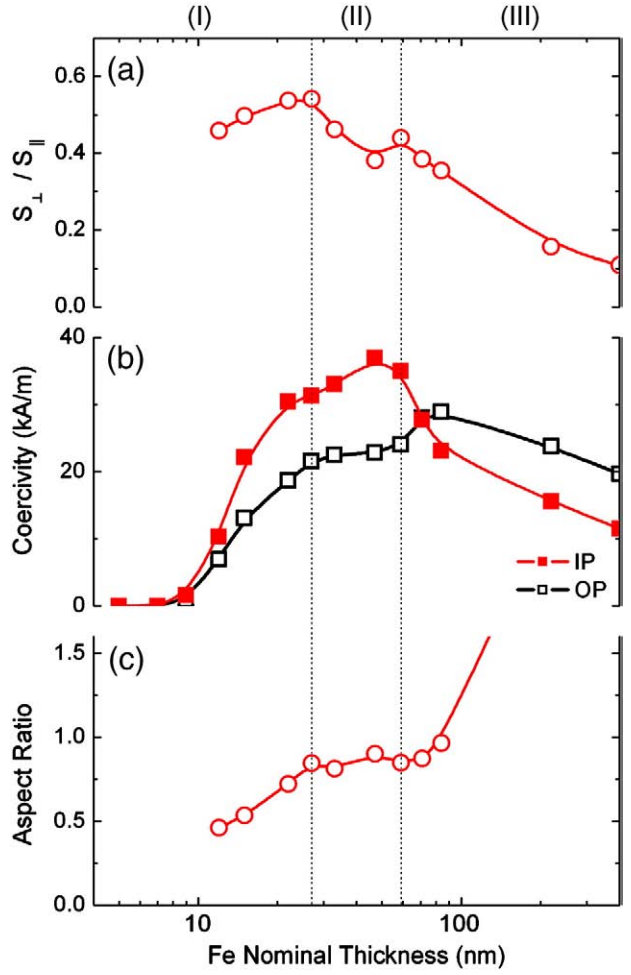

Fig. 3. (a) $S_\perp/S_\parallel$, (b) in-plane (IP) and out-of-plane (OP) coercivity, and (c) aspect ratio of nano-size Fe arrays with various nominal thicknesses.

volume (V). The magnetization, which anisotropy energy is overcome by the thermal fluctuation being randomized, becomes unstable. Therefore, the coercivity decreases. In Fig. 3(b), a maximum in-plane coercivity of up to 38 kA/m is achieved for $\tau_n = 47$ nm as the Fe nominal thickness decreases from $\tau_n = 400$ nm. This indicates that a nano-size Fe array below $\tau_n = 47$ nm with a diameter of about 52 nm is a single-domain array. Therefore, in the single-domain region, we suggest that the magnetization reversal of the 3-D random mode, the easy direction of which is assigned in spherical random, is shown for $\tau_n < 27$ nm, and changes to that of the 2-D random mode, the easy direction of which is in planar random, as the magnetostatic and exchange interactions increase [19].

The magnetic properties mentioned above are influenced by the nominal thickness or even the morphology of the Fe arrays. In Fig. 3, the results are divided into three regions of specific magnetic properties with various Fe nominal thicknesses. In region (I) for $\tau_n < 27$ nm, the magnetization reversal of nano-size Fe arrays that is initially formed is obviously influenced by the thermal effect [18]. The higher ratio of $S_\perp/S_\parallel$ is found to be related to the thermal fluctuation, which leads to randomized magnetization. In region (II) for $27\text{ nm} < \tau_n < 59$ nm, the ratio of $S_\perp/S_\parallel$ drops due to a reduced effect of the thermal fluctuation; as a result, the magnetization of nano-size Fe arrays tends toward the in-plane direction. The in-plane coercivity increases with the Fe nominal thickness until the critical dimension of the single domain, but the out-of-plane coercivity remains almost constant. Due to the lower exchange length of Fe (5.8 nm) [20] and the lower aspect ratio of the array (nominal thickness/diameter ~1, shown in Fig. 3(c)), this in-plane flower state is also supported by Ref. [4]. For $\tau_n > 59$ nm, the arrays become interconnected and act as a continuous film magnetically, named region (III). The adjacent arrays suppress the increase in diameter, causing the aspect ratio of the array to be enhanced rapidly with increases in the Fe nominal thickness [21]. Moreover, the pores, surrounded by the interconnected arrays, are thus formed, causing a pinning effect that slightly enhances the tendency of the ratio of $S_\perp/S_\parallel$ [22,23]. This mechanism is caused by the surface roughness, which tilts the magnetization away from the easy direction in the multi-domain region. In terms of micromagnetic theory, the coercivity should be enhanced by the non-magnetic defect with a size smaller than the domain wall width of the magnetic matrix [24]. For the Fe examined in this study, the typical material parameter of domain wall width is about 30 nm [17,18,20]. However, no obviously enhanced tendency in the in-plane coercivity is observed in region (III) of Fig. 3(a). It could be that the maximum coercivity is achieved for $\tau_n = 47$ nm; this tendency, caused by the pinning effect, may be overlapped. Finally, as the pores are covered up, which happens as the Fe nominal thickness increases without any discernable pinning effect, domain wall motion is promoted, leading to the decreases in in-plane and out-of-plane coercivity. The ratio of $S_\perp/S_\parallel$ is reduced gradually, resembling that of a continuous film.

In Fig. 4, the angular variation of coercivity of nano-size Fe arrays with various nominal thicknesses, normalized with respect to the coercivity of the easy direction, is measured as a function of applied field angle from in-plane (0°) to out-of-plane (90°). The angular variation of coercivity can provide information to determine the magnetization reversal mechanisms [25,26]. The result of domain wall motion should follow the Kondorsky relation [27]:

$$\cos\theta = H_c(0) / H_c(\theta), \tag{1}$$

where θ is the angle between the easy direction and the applied field. Therefore, the curve of domain wall motion is plotted as the coercivity on θ proportion to $1/\cos\theta$ as the upper limit, as shown in Fig. 4. The curves of larger Fe nominal thickness for $\tau_n = 400$, 220, and 84 nm are close to the curve of domain wall motion, indicating that the magnetization reversal is dominated by domain wall motion. It also

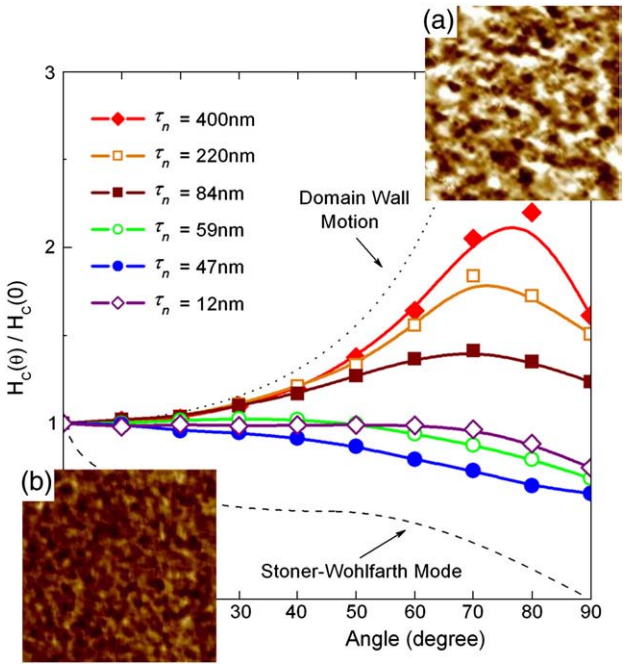

Fig. 4. Angular variation of coercivity of nano-size Fe arrays with various nominal thicknesses. The insets are the corresponding MFM images under a zero-field state with various nominal thicknesses of (a) 400 nm and (b) 47 nm. The scanning size of the images is 2 μm × 2 μm.

demonstrates the larger coercivity in the out-of-plane direction than that in the in-plane direction in region (III) of Fig. 3(b). As the Fe nominal thickness decreases to 47 nm, the morphology changes from continuous film to isolated arrays, and magnetostatic and exchange interactions decrease. The magnetization reversal of domain wall motion is gradually diminished, turning into that of the spin rotation, or so-called Stoner-Wohlfarth mode [28]. The curves are close to this lower limit, as shown in Fig. 4. However, for τ_n<47 nm, e.g. τ_n = 12 nm, the curve is flattened instead, verifying the variation of magnetization reversal from 2-D (planar) to 3-D (spherical) random mode [29]. The tendency of the curves can also be estimated by the difference between in-plane and out-of-plane coercivity, which is reduced for τ_n<47 nm, as shown in Fig. 3(b). The insets of Fig. 4 are MFM images with τ_n = 47 nm and 400 nm. These two insets show that the interaction of the Fe arrays increases with the Fe nominal thickness, resulting in the decrease in the average domain size. Furthermore, for τ_n<47 nm, the predominant dipolar interaction is identified by Henkel plot (not shown here), verifying the decrease in exchange interaction. For application in storage, the magnetization reversal of the spin rotation, which is preferable to that of the domain wall motion, facilitates the reduction of media noise [30].

In this study, the magnetization reversal of nano-size Fe arrays is size-dependent. The intrinsic coercivity of single-domain Fe spherical particles is equal to $2\,K_1/M_s = 2\,(4.5\times10^5/1714) = 525$ Oe (42 kA/m), where K_1 is the anisotropy constant and M_s is saturation magnetization [17]. As shown in Fig. 3, the maximum coercivity of about 38 kA/m is achieved as the aspect ratio of the array of about 0.9 approaches 1. The less but nearly identical value in coercivity verifies the negligible extrinsic shape anisotropy and the predominant contribution in the intrinsic crystal anisotropy. Otherwise, for the magnetization reversal, the coherent rotation is defined as all spins remaining parallel to one another during rotation and not remaining parallel in incoherent rotation. For Fe, the critical diameter of coherent rotation is calculated to be about 17 nm for spherical particles and 12 nm for infinite cylinders [17]. Paulus et al. [31] estimated the critical diameter of infinite Fe cylinders theoretically to be equal to $\pi^{1/2}\times\lambda_w$, where λ_w is the domain wall width. The domain wall width, λ_w, is equal to $2\,(A/K_s)^{1/2}$, where A and K_s are the exchange and shape anisotropy constants, respectively. For Fe nanowire, using the values $A = 1\times10^{-6}$ erg/cm and $K_s = 9.51\times10^6$ erg/cm^3, the critical diameter should be about 11.5 nm. However, for τ_n<27 nm with a diameter of lower than about 32 nm, the magnetization reversal is influenced by the thermal effect in practice. Regardless of the theoretical values of critical diameter mentioned above, it is just in this effect region of the thermal fluctuation. Therefore, the critical diameter of coherent rotation could not be estimated in this experiment. This may verify that coherent rotation is the ideal case in magnetization reversal.

4. Conclusions

We have fabricated large area, vertically aligned nano-size Fe arrays on the top of AAO templates and analyzed the size-dependent magnetization reversal. In the single-domain region, the magnetization reversal of the 3-D random mode is verified for τ_n<27 nm, and changed to the 2-D random mode as the Fe nominal thickness increases, resulting from the increasing anisotropy energy, showing the in-plane anisotropy. The increase in Fe nominal thickness results in a change in variation of morphology from isolated to interconnected, leading to the increased magnetostatic and exchange interactions. The pinning effect is also found in the multi-domain region before the pores are covered. The fundamental magnetization reversal could be developed for high crystal anisotropy materials and smaller dimensions of AAO templates. Such developments would be potentially applicable to future storage applications.

Acknowledgements

This work was financially supported by the National Science Council of Taiwan and Ministry of Economic Affairs of Taiwan through Grant Nos. NSC 98-2112-M-030-002 and 97-EC-17-A-08-S1-006, respectively. We would like to express our gratitude for the use of the facilities of the Core Facilities for Nanoscience and Nanotechnology at Academia Sinica.

References

[1] K. Liu, J. Nogues, C. Leighton, H. Masuda, K. Nishio, I.V. Roshchin, I.K. Schuller, Appl. Phys. Lett. 81 (2002) 4434.
[2] C. Kim, T. Loedding, S. Jang, H. Zeng, Z. Li, Y. Sui, D.J. Sellmyer, Appl. Phys. Lett. 91 (2007) 172508.
[3] T. Seki, T. Shima, K. Yakushiji, K. Takanashi, G.Q. Li, S. Ishio, J. Appl. Phys. 100 (2006) 043915.
[4] C.A. Ross, M. Hwang, M. Shima, J.Y. Cheng, M. Farhoud, T.A. Savas, H.I. Smith, W. Schwarzacher, F.M. Ross, M. Redjdal, F.B. Humphrey, Phys. Rev. B 65 (2002) 144417.
[5] H. Wang, Y.C. Wu, L. Zhang, X. Hu, Appl. Phys. Lett. 89 (2006) 232508.
[6] B.C. Lim, J.S. Chen, J.F. Hu, Y.K. Lim, B. Liu, G.M. Chow, G. Ju, J. Appl. Phys. 103 (2008) 07E143.
[7] Y.H. Fang, P.C. Kuo, P.L. Lin, S.C. Chen, C.T. Kuo, G.P. Lin, J. Magn. Magn. Mater. 320 (2008) 3032.
[8] D.H. Wei, F.T. Yuan, H.W. Chang, K.L. You, Y. Liou, T.S. Chin, C.C. Yu, Y.D. Yao, Nanotechnology 18 (2007) 335603.
[9] J.J. Lin, T. Zhang, P. Lee, S.V. Springham, T.L. Tan, R.S. Rawat, T. White, R. Ramanujan, J. Guo, Appl. Phys. Lett. 91 (2007) 063120.
[10] Y.F. Ding, J.S. Chen, B.C. Lim, J.F. Hu, B. Liu, G. Ju, Appl. Phys. Lett. 93 (2008) 032506.
[11] M.T. Rahman, N.N. Shams, Y.C. Wu, C.H. Lai, D. Suess, Appl. Phys. Lett. 91 (2007) 132505.
[12] C.Y. Kuo, S.Y. Lu, T.Y. Wei, J. Cryst. Growth 285 (2005) 400.
[13] Kai-Tze Huang, Po-Cheng Kuo, Yeong-Der Yao, Thin Solid Films 517 (2009) 3243.
[14] Y. Lei, W.K. Chim, Chem. Mater. 17 (2005) 580.
[15] T. Karabacak, T.M. Lu, J. Appl. Phys. 97 (2005) 124504.
[16] S.P. Li, W.S. Lew, Y.B. Xu, A. Hirohata, A. Samad, F. Baker, J.A.C. Bland, Appl. Phys. Lett. 76 (2000) 748.
[17] B.D. Cullity, Introduction to Magnetic Materials, Addison-Wesley, Reading, Massachusetts, 1972.
[18] D. Weller, A. Moser, IEEE Trans. Magn. 35 (1999) 4423.
[19] G.F. Hughes, J. Appl. Phys. 54 (1983) 5306.
[20] M.E. Schabes, J. Magn. Magn. Mater. 95 (1991) 249.
[21] H. Zheng, J. Zhong, W. Wang, Y. Zheng, C. Ma, Thin Solid Films 516 (2008) 4983.
[22] T.H. Wu, J.C. Wu, B.M. Chen, H.P.D. Shieh, J. Magn. Magn. Mater. 202 (1999) 62.
[23] M.T. Rahman, C.H. Lai, D. Vokoun, N.N. Shams, IEEE Trans. Magn. 43 (2007) 2133.
[24] R.C. O'Handley, Modern Magnetic Materials, John Wiley & Sons, New York, 2000.
[25] D.Y. Oh, J.K. Park, J. Appl. Phys. 97 (2005) 10N105.
[26] X. Bao, F. Li, R.M. Metzger, J. Appl. Phys. 79 (1996) 4866.
[27] E. Kondorsky, J. Phys. USSR 2 (1940) 161.
[28] E.C. Stoner, E.P. Wohlfarth, Phil. Trans. R. Soc. A 240 (1948) 599.
[29] C. Byun, J. Sivertsen, J.H. Judy, IEEE Trans. Magn. 22 (1986) 1155.
[30] S. Iwasaki, K. Ouchi, N. Honda, IEEE Trans. Magn. 16 (1980) 1111.
[31] P.M. Paulus, F. Luis, M. Kröll, G. Schmid, L.J. de Jongh, J. Magn. Magn. Mater. 224 (2001) 180.